applied sciences

MDPI

Article

Optimization of Buoy Shape for Wave Energy Converter Based on Particle Swarm Algorithm

Wei Ge [1], Shui Ji [1], Yeqing Jin [2,*], Shijie He [2], Hailong Chen [2] and Hengxu Liu [2]

[1] State Power Investment Company Science and Technology Research Institute, Beijing 102209, China; gewei@spic.com.cn (W.G.); jishui@spic.com.cn (S.J.)
[2] Yantai Research Institute and Graduate School, Harbin Engineering University, Yantai 265500, China; heshijie@hrbeu.edu.cn (S.H.); chenhailong@hrbeu.edu.cn (H.C.); liuhengxu@hrbeu.edu.cn (H.L.)
* Correspondence: jinyeqing@hrbeu.edu.cn

Abstract: In order to improve the wave energy capture rate of the buoy of a wave energy generation device, this paper proposes a multi-degree of freedom method to optimize the shape of the buoy with maximum wave energy capture. Firstly, a multi-degree of freedom wave energy converter was designed, and the buoy shape was defined using a B-spline curve to generate the shape vector; then, a numerical model of the multi-degree of freedom wave energy converter was established and numerical calculations were carried out using AQWA/WEC-Sim software; on this basis, the particle swarm optimization algorithm was introduced to find the buoy shape corresponding to the maximum wave energy capture. Finally, the optimization of the buoy shape was in irregular waves. The results show that as the wave energy capture increased, the buoy shape tended to be flatter, with a smaller taper, and the optimal buoy shape had a better motion response than the conventional cone buoy. Eventually, the correctness of the buoy shape optimization method was verified through experimental testing.

Keywords: particle swarm optimization; wave energy converter; buoy-shape; multi-degree of freedom; B-spline curve

Citation: Ge, W.; Ji, S.; Jin, Y.; He, S.; Chen, H.; Liu, H. Optimization of Buoy Shape for Wave Energy Converter Based on Particle Swarm Algorithm. *Appl. Sci.* **2024**, *14*, 1889. https://doi.org/10.3390/app14051889

Academic Editors: Yingyi Liu, Rongquan Wang and Robert Mayon

Received: 30 January 2024
Revised: 21 February 2024
Accepted: 22 February 2024
Published: 25 February 2024

1. Introduction

With the development of the world economy, the demand for energy consumption is increasing and the world's energy shortage is driving the development of new energy technologies and innovations. In order to achieve sustainable development, China is actively promoting a 'carbon peaking and carbon neutrality' energy policy. In this context, wave energy converters (WECs) based on offshore stationary wind turbines have become an important and promising research area. Offshore stationary wind turbines have the advantage of a fixed structure and high wind energy efficiency, while WECs can effectively harness the energy of waves. By combining these two technologies, not only can the energy output per unit of ocean area and the stability of power output be improved but also the mooring, transmission, and distribution costs of wave power generation devices can be eliminated, which can achieve the goal of the diversification and sustainable development of green energy and provide strong support for China to achieve the 'carbon peaking and carbon neutrality goals'. The aim of this paper is to address the bottleneck issue faced by enterprises and provide a new technological pathway for designing high-performance buoys, thereby offering a novel approach for the design of buoy shapes for multi-degree-of-freedom WECs.

At present, most of the research on WEC technology is focused on primary energy conversion, secondary energy conversion [1], and the spatial arrangement of power plants [2]. Specifically, these include the optimization of buoy hydrodynamic characteristics, efficient and stable energy conversion, and arrayed power plants. It has been shown that improvements to the buoy shape and structure can improve its hydrodynamic performance [3],

which is important for improving the efficiency of primary energy conversion. Therefore, buoy shape optimization has become one of the hot topics in WEC primary energy conversion research.

In terms of primary energy conversion, this study can be broadly based on the definition of buoy geometry, numerical calculation methods, and the selection of optimization algorithms. For example, buoy geometry is defined using B-spline surfaces [4–7], Bézier curves [8], specific shapes such as rectangles and wedges [9,10], changing the outer diameter and bottom shape of the buoy [11], using polar equations in polar coordinates [12], and changing other parameters while keeping the buoy volume constant [13]. A complex buoy shape is also defined by a central line and multiple cubic B-spline curves [14]. In terms of numerical calculation methods, there are joint simulations by AQWA/WEC-Sim boundary element methods [15–17] for numerical calculations. Nazari et al. [18] used AQWA to calculate hydrodynamic data for different buoy shapes, followed by MATLAB codes to obtain output power and efficiency. Similarly, the hydrodynamic data were calculated by AQWA software and then the design of experiments method was applied by Minitab software [19] to determine the optimum geometry. The Taguchi design and response surface design methods [20,21] were used to develop a shape optimization process, also using computational fluid dynamics software for viscous hydrodynamic calculations [10,22]. In terms of optimization using metaheuristic algorithms, in previous studies, genetic algorithms have been used to develop multi-objective problems [23,24]. Amini et al. [25] used five metaheuristic algorithms to achieve the optimal value of WEC power output under damping. Garcia et al. [6] used the genetic algorithm and the particle swarm optimization algorithm (PSO) to propose different geometry definition methods adapted to different optimization algorithms. Song et al. [26] proposed a PSO-based heuristic framework for solving nonlinear continuous maximum coverage position models. He et al. [27] proposed the effect of buoy volume on power capture based on a differential evolutionary algorithm. Lin et al. [14] used a genetic algorithm combined with a neural network to determine optimal buoy shape, and the implementation of a neural network greatly reduced the computation time. Liu et al. [28] proposed a buoy shape optimization method based on an annual average power prediction model by combining a multi-island genetic algorithm and a power prediction model. In the field of secondary energy conversion, the processes are mainly hydraulic, electromagnetic direct-drive, mechanical direct-drive [29], etc. Due to the general low frequency of waves, direct-driven wave energy conversion is not efficient for power generation. Baninajar et al. [30] proposed a dual-stack coaxial magnetic gear to improve the energy output efficiency of a generator and Liu et al. [31] proposed a permanent magnet-induction magnetic screw with high thrust density and high energy conversion efficiency to improve the energy conversion efficiency of direct-drive electromagnetic processes. Calvário et al. [32] proposed a technique to match the geometric and control parameters of a power take-off (PTO) system for a WEC using a genetic algorithm to increase the excitation torque of the buoy and improve the conversion efficiency of the PTO system. Fan et al. [33] proposed a hydraulic WEC combined with an offshore wind turbine, and a fuzzy controller was designed to regulate the displacement of the hydraulic motor and control the output power. Geng et al. [34] proposed a new hydraulic PTO power regulation module structure to improve the power output stability of the hydraulic PTO under irregular wave conditions. In the field of power plant array arrangement, Veurink et al. [35] proposed a cost function to optimize the array arrangement of a WEC, with the aim of minimizing power variation and energy storage while maximizing the energy delivered to onshore points co-coupled with the grid. de Andrés et al. [36] studied the coefficients influencing the layout of wave energy field arrays, such as the number of WECs and wave directionality. Stratigaki et al. [37] conducted experimental studies by means of design trials for a range of geometric layout configurations and wave conditions.

Through an analysis of the current research status at home and abroad, it has been found that although defining the geometric shape of buoys using methods such as Bézier curves or B-spline surfaces can achieve optimal energy harvesting efficiency, it sacrifices

the manufacturability of the buoys. This is because buoy shapes that are symmetric and regular are more suitable for engineering applications. Defining specific shapes to describe buoy shapes and optimizing buoy shapes using computational fluid dynamics methods presents challenges such as high computational complexity and scalability issues. Similarly, using metaheuristic algorithms for buoy optimization also has limitations. For example, optimizing buoy shapes typically involves a large number of design variables, leading to a large search space. Some algorithms may also exhibit slow convergence rates, especially when dealing with complex problems, requiring long search times to achieve satisfactory solutions.

The proposed method defines the geometric shape of the buoy through a 5-dimensional shape vector based on B-spline curves, while enforcing constraints on the coordinate parameters' upper and lower limits, ensuring that the buoy's shape remains regular throughout the optimization process. In terms of model development, compared to conventional computational fluid dynamics buoy shape optimization methods, the unique modeling tool of WEC-Sim empowers this method with the capability to develop multi-degree-of-freedom WECs. Due to the introduced PSO's capability to search for the global optimal solution within the population, it does not require the computation of gradients or derivatives. Therefore, it can effectively handle problems without explicit expressions or continuity. Compared to traditional optimization methods such as gradient descent, the implementation of PSO is relatively simple. It does not require a complex problem framework; rather, it only necessitates the definition of appropriate fitness functions and parameter settings. Additionally, PSO is less sensitive to the choice of initial conditions and parameter settings, typically exhibiting good robustness. As a result, it provides a more comprehensive exploration of operating conditions compared to conventional optimization methods, leading to more precise solutions.

The structure of this paper is as follows: Section 1 provides the introduction, Section 2 presents the theory of hydrodynamic calculations and optimization methods, Section 3 analyzes the evolutionary patterns of buoy shapes under irregular waves, Section 4 is dedicated to experimental verification, and, finally, the conclusion of the entire paper is given.

2. Theory and Methodology

2.1. Numerical Model

Successful international wind and wave co-generation devices, such as the semi-submersible triangular wind and wave energy hybrid system W2Power developed by Wave energy in Norway and the Wave Star basic array WEC developed in Denmark, are all WEC built on ocean platforms. The efficiency of the WECs varies depending on the coupling to the ocean platform. In this paper, a three-dimensional diagram of a WEC based on an offshore fixed wind turbine is shown in Figure 1.

The above 3D model is simplified to obtain a schematic diagram of the operation of a single buoy coupled to a wind turbine. As shown in Figure 2, for this multi-degree of freedom WEC, there are two rotational joints, located at the beginning and end of the pendulum arm, with one end connected to the buoy and the other to the turbine base. H is the distance from the buoy restraint point to the PTO articulation point, h_1 is the distance from the buoy center to the restraint point, h_2 is the distance from the PTO articulation point to the upper surface of the buoy, and D is the tower diameter. In the time domain analysis, two rotational joints were established. The rotational joint connected to the tower incorporated the entire pendulum system to establish a rotating PTO system, with a damping coefficient C_{PTO} to generate electrical energy output. A rotational constraint was set at the rotational joint connecting the buoy and the swing arm, with a damping coefficient C.

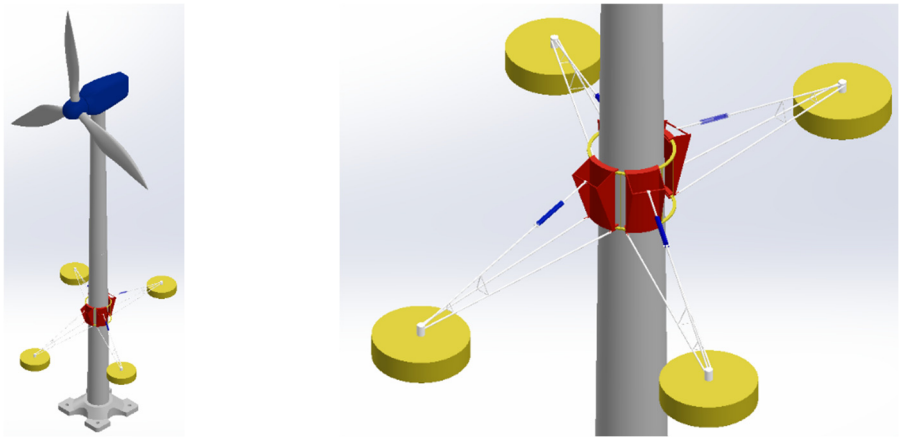

(**a**) (**b**)

Figure 1. Three-dimensional model of wind and wave combined device: (**a**) modelling diagram; (**b**) Partial enlargement diagram.

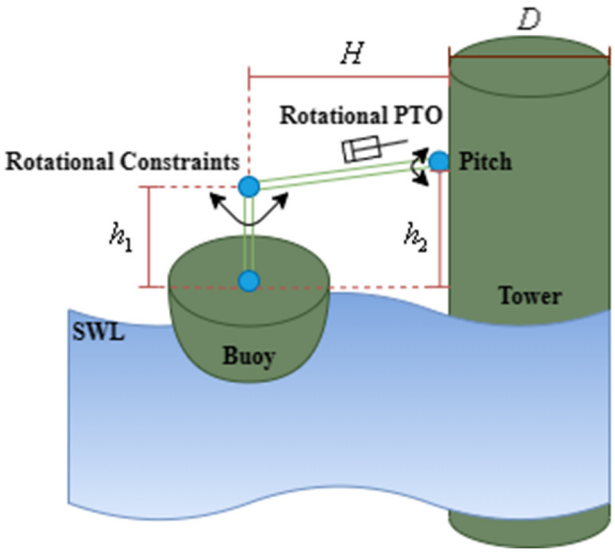

Figure 2. Schematic representation of WEC in pitch motion.

2.2. Hydrodynamic Theory

According to Newton's second law, the equation of motion of a swing arm wave energy buoy in the frequency domain can be obtained as follows:

$$\left[-iw(M + M_{add}) + \lambda - \frac{K}{iw}\right]\zeta = F_{exc} \tag{1}$$

where M is the wave energy buoy mass, K is the restoring force coefficients, and ξ is the motion response amplitude.

Once the frequency domain equation of motion of the wave energy buoy is obtained, the time domain equation of motion of the wave energy buoy can be found by inversion of the Fourier transform:

$$(M + M_\infty)\ddot{x}(t) + \int_0^t \dot{x}(\tau)h(t-\tau)d\tau + Kx(t) = F_{exc}(t) \tag{2}$$

where M_∞ is the additional mass of the buoy at infinity and $h(t)$ is the time delay function, which can be expressed as

$$h(t) = \frac{2}{\pi}\int_0^\infty \lambda(w)\cos wtdt \tag{3}$$

where $\lambda(\omega)$ is the radiation damping function.

For a particular swing-arm WEC with a PTO system, the equation of motion in the time domain can be expressed as

$$(J + J_\infty)\ddot{\theta}(t) + Kl\theta(t) + l\int_0^t h(t-\tau)\dot{\theta}(\tau)d\tau = M_{exc}(t) + M_{PTO}(t) \tag{4}$$

where l is the equivalent length of the arm, $M_{PTO}(t)$ is the linear PTO damping moment, $M_{exc}(t)$ is the excitation moment, J and J_∞ are the rotational inertia of the buoy and the additional rotational inertia at infinity, and $\theta(t), \dot{\theta}(t), \ddot{\theta}(t)$ are the oscillation angle, angular velocity, and angular acceleration of the system, respectively.

The linear PTO damping moment is expressed as

$$M_{PTO}(t) = -C_{PTO}\dot{\theta}(t) \tag{5}$$

where C_{PTO} is the damping of the system.

The instantaneous energy capture power of the device is

$$P_{in}(t) = M_{PTO}(t)\dot{\theta}(t) \tag{6}$$

The average energy capture power of the device from time t_1 to t_2 is

$$P_{in} = \frac{1}{t_2 - t_1}\int_{t_1}^{t_2} P_{in}(t)dt \tag{7}$$

Therefore, the designed WEC system can be analyzed by the force analysis revealed in Figure 3.

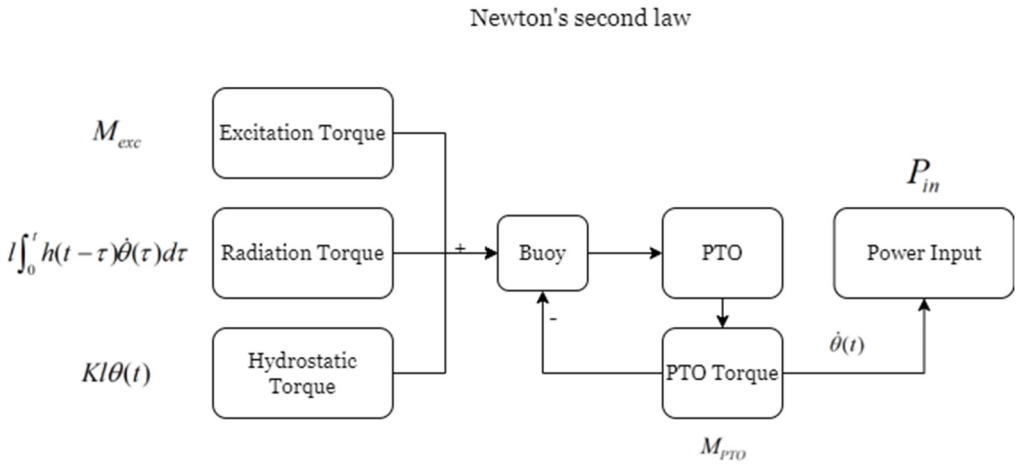

Figure 3. The torque composition analysis of the swing-arm WEC.

2.3. Optimization Methods

In this study, a multi-degree of freedom time domain model was jointly developed using AQWA/WEC-Sim. AQWA is a dedicated simulation tool for the marine and offshore engineering industry and is commonly used to calculate hydrodynamic problems related to ships and offshore engineering. The classical interface of AQWA requires parametric modeling in APDL to provide the input files for AQWA. WEC-Sim is an open-source code

for simulating WECs, developed in MATLAB/SIMULINK using the multibody dynamics solver Simscape Multibody. WEC-Sim is capable of modeling devices consisting of hydrodynamic rigid bodies, articulations and constraints, PTO systems, and mooring systems. Simulations are performed in the time domain by solving the equations of motion of a controlled WEC with six rigid Cartesian degrees of freedom.

The optimization method can be divided into the following steps:

(1) Generate shape vectors by the buoy shape definition method.
(2) Input the variables into ANSYS APDL for parametric modeling, generate the hydrodynamic suffix dat file, put the dat file into AQWA for calculation, and obtain the suffix ah1 file and lis file. (These two files are the hydrodynamic input files of WEC-Sim, generated by the internal Bemio function with the suffix h5 file, and the h5 file is the final WEC-Sim calculation file.) Calculate the target function fitness values by WEC-Sim.
(3) Introduce the optimal PSO, compare the objective function fitness values, generate new variables, and then repeat steps (1) and (2). When the fitness value, which is the within-iteration best value of the population, remains unchanged or changes by less than a certain threshold, and the maximum number of iterations set has been reached, the algorithm is considered to have converged.

Optimization algorithms are divided into traditional and intelligent algorithms. Traditional optimization algorithms are deterministic algorithms with fast convergence and a definite termination criterion, but the solution results are strongly dependent on the initial values and only locally optimal solutions can be obtained, such as linear programming and constraint methods. In order to avoid getting trapped in a local optimum, it is recommended to use intelligent optimization algorithms that can search for the global optimum, such as PSO and simulated annealing methods. This paper focuses on the optimization of buoy parameters using PSO because of their simplicity and ease of implementation with few parameters.

A simplified algorithmic model was first proposed by James Kennedy and Russell Eberhart in 1995 [38]. This model focused on bird foraging behavior, where flocks of birds shared information about the group to find the best foraging site. PSO has been refined over the years.

In buoy shape optimization, the position of each particle not only represents a candidate solution but also contains information about the shape of the buoy. Specifically, each candidate solution can be represented as a vector, where each element represents the shape characteristics of the buoy in different dimensions, such as length, diameter, etc. In the PSO algorithm, the position of each particle is the shape vector of a buoy, and the update process is adapted to update the elements of the shape vector accordingly.

In the PSO algorithm, the velocity and position of each particle can be updated using the following equations:

$$\begin{cases} v_{id}^{k+1} = wv_{id}^{k} + c_1 r_1 (p_{id,pbest}^{k} - x_{id}^{k}) + c_2 r_2 (p_{d,gbest}^{k} - x_{id}^{k}) \\ x_{id}^{k+1} = x_{id}^{k} + v_{id}^{k+1} \end{cases} \tag{8}$$

where $i \in 1, 2, \cdots N$, N is the number of particles, $d \in 1, 2, \cdots G$, G is the number of particle dimensions, k is the number of iterations, $r_1, r_2 \in [0,\ 1]$, c_1, c_2 are the individual learning factor and the population learning factor, respectively, ω is the inertia weights, x_{id}^{k} is the position of the *i-th* particle in the *d-th* dimension in the *k-th* iterations, v_{id}^{k} is the velocity of the *i-th* particle in the *d-th* dimension in the *k-th* iterations, $p_{id,pbest}^{k}$ is the historical optimal position of the *i-th* particle in the *d-th* dimension after the *k-th* iterations, and $p_{d,gbest}^{k}$ is the historical optimal position of the population in the *d-th* dimension after the *k-th* iterations.

Based on the above introduction to the PSO algorithm, the pseudocode of the PSO is revealed in Figure 4.

```
Initialize the population of particles with random positions and velocities
Initialize the best-known positions of each particle
Initialize the global best-known position
Set maximum number of iterations or a termination criterion

While termination criterion is not met:
    For each particle:
        Evaluate the fitness of the current position
        If the current position is better than the best-known position:
            Update the best-known position of the particle
        If the current position is better than the global best-known position:
            Update the global best-known position

    For each particle:
        Update the velocity using the formula:
            velocity(t+1) = inertia * velocity(t) + c1 * rand() * (best_known_position -
current_position) + c2 * rand() * (global_best_known_position - current_position)
        Update the position using the formula:
            position(t+1) = position(t) + velocity(t+1)

    Increment the iteration counter

End While

Return the global best-known position
```

Figure 4. PSO algorithm pseudocode.

The following Table 1 shows the parameter settings of the PSO.

Table 1. Parameters of PSO.

Parameters	Value
i	30
d	5
k	20
ω	0.6
c_1	1.6
c_2	1.8
v_{max}	(0.135, 0.075, 0.15, 0.075, 0.15)

The number of particles [39] is typically between 20 and 1000, with a range of 20 to 40 being suitable for simple problems. A smaller population size may lead to getting trapped in local optima, while increasing the number of particles can enhance convergence speed, allowing for faster discovery of the global optimum. However, a larger population size also entails increased computational costs per iteration. For this study, a population size of 30 seemed appropriate. The shape vector consisted of 5 variables, corresponding to a dimensionality of 5. The number of iterations usually depends on the difficulty of the question; it needs to be adjusted according to the actual situation in the process of optimization. Due to the significant computational burden and file modifications involved in the joint simulation in this study, a value of 20 iterations was deemed appropriate. The inertia factor [40,41] typically ranges from 0.4 to 2, while the acceleration factor [42] typically ranges from 0 to 4. Choosing intermediate values is generally suitable. v_{max} refers to the maximum velocity of the particle; it was set to 10~20% of the particle variation range. The range of variation of the particles is shown in Equation (9).

The above steps allow for the use of the PSO algorithm for buoy shape optimization to find the global optimal solution. The specific technical path is shown in Figure 5.

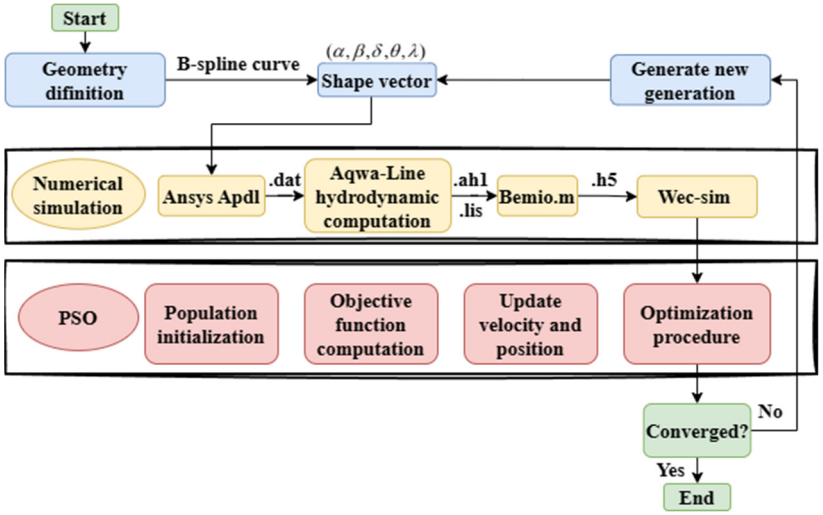

Figure 5. Buoy shape optimization flow chart for the PSO algorithm.

For the PSO, the value of the fitness was calculated by substituting the vector into a specific objective function, which was chosen to determine the shape of the buoy. In recent years, the technical challenges of wave power generation have focused on efficient energy conversion technology and the optimization of the hydrodynamic performance of buoys. The buoy captures waves for primary energy conversion, which is related to the hydrodynamic performance of the buoy, while the secondary energy conversion depends on the mechanical structure and the method of energy conversion. Therefore, how to improve the energy capture capacity of the buoy is the key. Therefore, the objective function could be defined as the average power captured by the buoy in a wave, represented by P_{in}. By calculating and comparing the value of the objective function, the average power captured by the buoy was maximized for a given wave condition.

When the PSO was applied to the buoy line optimization problem, the particles of the PSO were selected as the coordinates of the control vertex X_1, X_2, X_3, X_4, X_5 of the B-spline curve that controlled the shape of the buoy, which formed the shape vector $(\alpha, \beta, \delta, \theta, \lambda)$. As shown in Figure 6, β controlled the buoy draft height, δ, θ, β jointly controlled the buoy draft volume, λ controlled the buoy waterline cross-sectional area, and α controlled the buoy bottom shape, with a maximum of 20 iterations. The shaded area enclosed by the B-spline curve and the x and z axes was rotated 360° about the axis of rotation z, which was the shape of the buoy below the surface line. The upper and lower bounds were set to 15–20% of the difference between the upper and lower bounds so that the buoy shape was not unreasonably sharp or concave, and the algorithm was restricted to search for the optimal solution within a certain range. The upper and lower bounds of the constraint can be expressed as

$$\begin{cases} 0 \le \alpha \le 1.0 \text{ m} \\ -1.5 \text{ m} \le \beta \le -1.0 \text{ m} \\ 1.0 \text{ m} < \delta \le 2.0 \text{ m} \\ -1.0 \text{ m} < \theta \le -0.5 \text{ m} \\ 2.0 \text{ m} < \lambda \le 3.0 \text{ m} \end{cases} \tag{9}$$

The equation of the B-spline curve can be expressed as

$$C(u) = \sum_{i=0}^{n} P_i N_{i,k}(u) \tag{10}$$

where $P_i (i = 0, 1, 2 \cdots n)$ are the control points—typically, there are $n + 1$ control points—and $N_{i,k} (i = 0, 1, 2 \cdots n)$ is the *k-th* B-spline basis function—the highest number of times

is k. The basis function is the k-th segmented polynomial determined by a node vector $[u_0, u_1 \cdots u_{n+k+1}]$. The nodes in the node vector are uniformly or equidistantly distributed along the parameter axes, and the B-spline curve is called a uniform B-spline curve. In this paper, a uniform 3rd-order B-spline curve was used to describe the buoy shape.

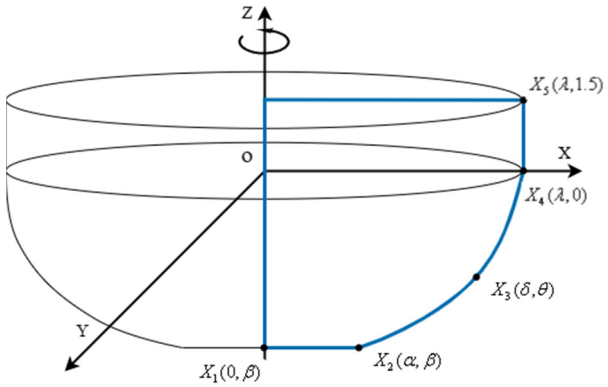

Figure 6. Geometry definition.

2.4. Validation

Due to the limitations of the AQWA software for time domain calculations of multi-degree-of-freedom models, this study performed hydrodynamic calculations of multi-degree-of-freedom models by combining the AQWA frequency domain and WEC-Sim time domain calculations numerically. In order to verify the correctness of the above method, the results computed by the combined AQWA/WEC-Sim were compared with those of Ruehl K et al [43]. Ruehl K et al used WAMIT to obtain the frequency domain hydrodynamic data and used WEC-Sim and Orca-flex software to perform time domain calculations for RM3 in a multi-degree-of-freedom model. In this study, the same models and settings were used for the comparison. The simulation model is presented in Figure 7.

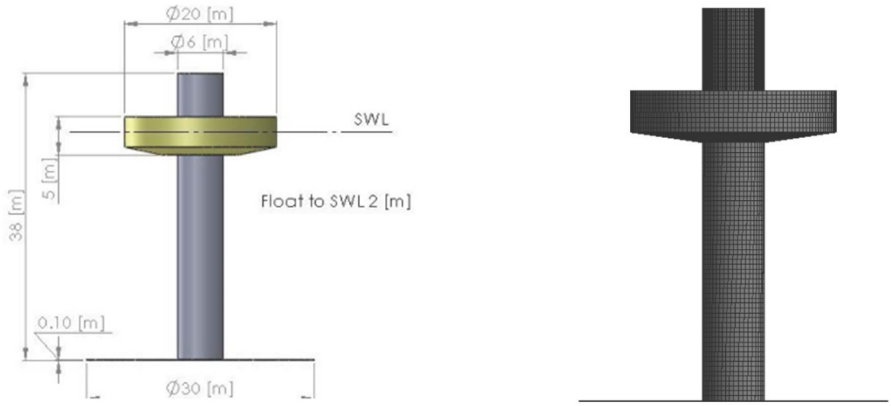

Figure 7. RM3 model: (**a**) geometric model from Ruehl K et al.; (**b**) grid model for AQWA frequency domain calculations in this paper.

The two models used the same wave conditions, and a regular wave with a wave height of 2.5 m and a period of 8 s was selected. As shown in Figure 8, the validated data from the literature are shown as blue lines and the data calculated by AQWA/WEC-Sim are shown as red lines. By comparing the pitch response curves of the RM3 device, it can be seen that the results of the method used in this paper are similar to those of the literature. The deviation of 0.02 deg was within the acceptable error range.

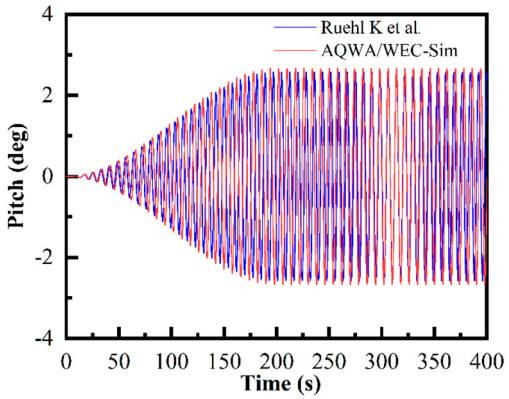

Figure 8. The simulation results compared with the results published by Ruehl K. et al. [43].

3. Results

In order to visualize the variation of power capture during the optimization of buoy shapes, irregular waves were calculated in the time domain to analyze the shape evolution and, finally, the hydrodynamic performance and energy capture capacity of the different buoys. The model parameters are shown in Table 2.

Table 2. System parameters of WEC.

Parameters	Value [m]
H	10
D	6.6
h_1	1.2
h_2	3.7

In order to simulate the hydrodynamic performance and shape optimization process of the buoy in real sea conditions, in this section, the improved JONSWAP wave spectrum proposed by Goda [44] is selected for numerical simulation, which can be used to generate irregular wave data according to the following wave spectrum equation. According to the theory of linear superimposition, irregular waves can be considered as the superposition of a large number of regular table lines with different periods, phases, and amplitudes.

$$S_f = \beta_J H_S^2 T_P^{-4} f^{-5} \exp\left[-\frac{5}{4}(T_P f)^{-4}\right] \cdot \gamma^{\exp\left[-(f/f_P-1)^2/2\sigma^2\right]} \tag{11}$$

$$\beta_J = \frac{0.06238}{0.230 + 0.0336\gamma - 0.185(1.9+\gamma)} \cdot [1.904 - 0.019151 \ln \gamma] \tag{12}$$

$$T_P = \frac{T_{H_S}}{1 - 0.132(\gamma + 0.2)^{-0.559}} \tag{13}$$

where H_S is the significant wave height, γ is the peak factor of the spectrum, f is the frequency, f_P is the peak frequency, σ is the peak type parameter, $\sigma = 0.07(\omega \leq \omega_P)$, $\sigma = 0.09(\omega > \omega_P)$, ω_P is the circular frequency at the spectral peak, and T_P is the peak period, which is equal to $1/f_P$.

Offshore wind farms are situated in the Yellow and Bohai Seas of China. Liang et al [45]. analyzed the wave heights and periods of the Chinese Yellow and Bohai Seas, so the most probable sea state was chosen for this paper. The spectral density function curves generated by the wave conditions are shown in Figure 9.

The above wave spectrum was simulated in WEC-Sim in the time domain; the WEC-Sim model is shown in Figure 10.

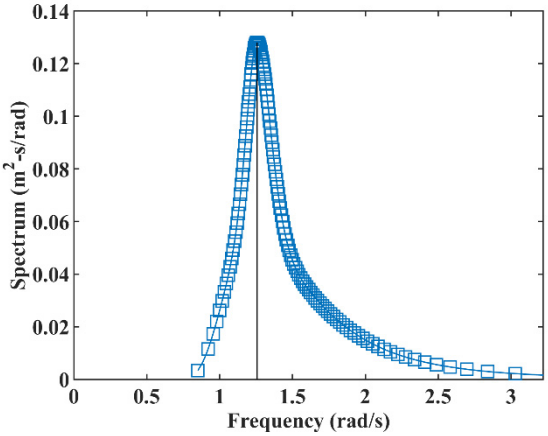

Figure 9. JS spectral density function curve.

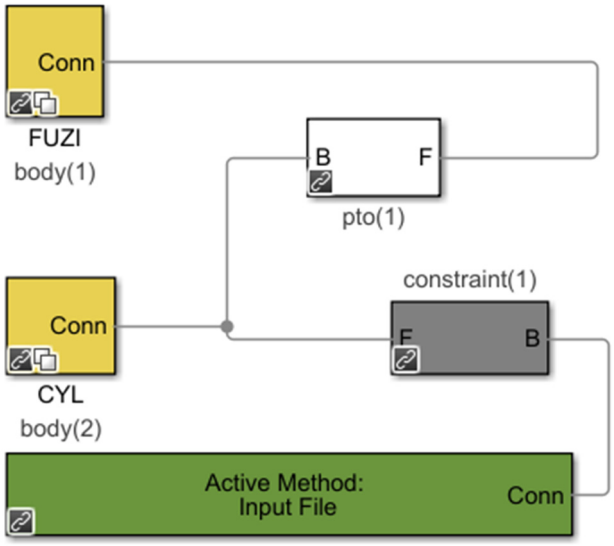

Figure 10. WEC-Sim model.

As shown in Figure 11, when *C* took 0, the objective function converged in 16 steps and the fitness value converged to 13.422 kW; when *C* took 5.0×10^5 Nms/rad, the objective function converged in 12 steps and the fitness value converged to 12.132 kW; when *C* took 1.0×10^6 Nms/rad, the objective function converged in 17 steps and the fitness converged to 12.390 kW. At the beginning of the iteration, the value of P_{in} was small and, as the iteration progressed, the motion response of the buoy gradually increased and the energy of the entire swing arm system was efficiently captured. Obviously, the fitness value of *C* was greater than that of the other two cases, and the power generation system worked in a more efficient energy capture range.

As shown in Figure 12, (a) is the motion response of the buoy in pitching degrees of freedom and (b) is the motion response of the system in pitching degrees of freedom. The maximum swing angle of the buoy was obtained when *C* took 0, the pitch angle reached 34 degrees, and, under the same damping coefficient, the swing angle of the system showed the same movement trend as the swing angle of the buoy, and the maximum swing angle of the system reached 9 degrees. In general, the motion response of the buoy affected the motion response of the system, and the more violently the buoy moved, the more violently the system swung.

Briefly, as shown in Tables 3–5, data from six representative iterations out of 20 were selected and had distinct characteristics.

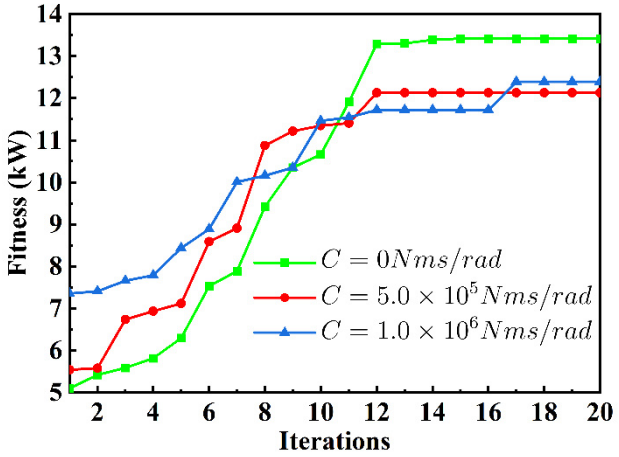

Figure 11. Iterative curve graph.

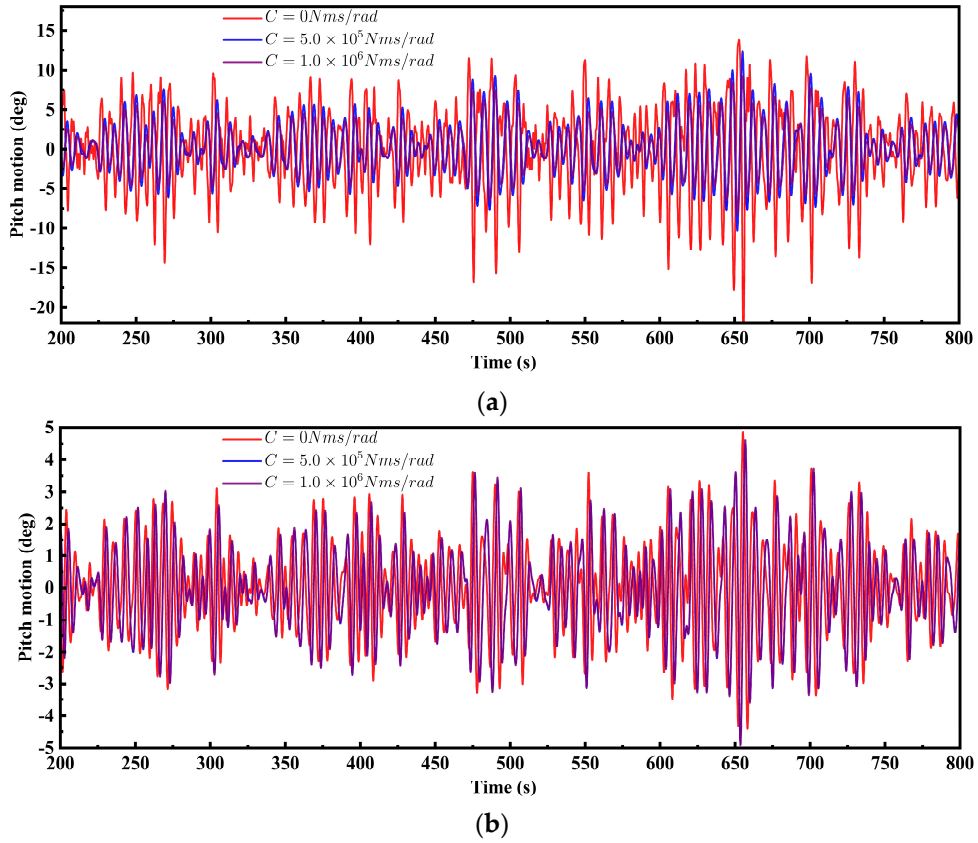

Figure 12. Motion response: (**a**) buoy pitch motion response; (**b**) swing-arm system pitch motion response.

Table 3. Results of $(\alpha, \beta, \delta, \theta, \lambda)$ for the iterations under $C = 0$.

Iterations	$(\alpha,\beta,\delta,\theta,\lambda)$ [m]	P_{in} [kW]
$k = 1$	(0.91, −1.4444, 1.3897, −0.798, 2.132)	5.1000
$k = 4$	(0.8004, −1.3856, 1.429, −0.7333, 2.2204)	5.8152
$k = 8$	(0.9476, −1.161, 1.4171, −0.63, 2.5984)	9.4225
$k = 12$	(1.0, −1.0, 1.3888, −0.5127, 2.9841)	13.300
$k = 16$	(1.0, −1.0, 1.3847, −0.5, 3.0)	13.422
$k = 20$	(1.0, −1.0, 1.3847, −0.5, 3.0)	13.422

Table 4. Results of $(\alpha, \beta, \delta, \theta, \lambda)$ for the iterations under 5.0×10^5 Nms/rad.

Iterations	$(\alpha,\beta,\delta,\theta,\lambda)$ [m]	P_{in} [kW]
$k = 1$	(0.6283, −1.3494, 1.2305, −0.9026, 2.1707)	5.5411
$k = 4$	(0.557, −1.3788, 1.5443, −0.9721, 2.3737)	6.9372
$k = 8$	(0.9204, −1.5, 1.3561, −1.0, 2.8379)	10.875
$k = 12$	(1.0, −1.5, 1.346, −1.0, 3.0)	12.132
$k = 16$	(1.0, −1.5, 1.346, −1.0, 3.0)	12.132
$k = 20$	(1.0, −1.5, 1.346, −1.0, 3.0)	13.132

Table 5. Results of $(\alpha, \beta, \delta, \theta, \lambda)$ for the iterations under 1.0×10^6 Nms/rad.

Iterations	$(\alpha,\beta,\delta,\theta,\lambda)$ [m]	P_{in} [kW]
$k = 1$	(0.1962, −1.1078, 1.2283, −0.7514, 2.3818)	7.3554
$k = 4$	(0.4423, −1.1048, 1.3199, −0.7351, 2.4343)	7.7898
$k = 8$	(0.7977, −1.0444, 1.3463, −0.5583, 2.7111)	10.156
$k = 12$	(0.9684, −1.0, 1.3521, −0.5, 2.9094)	11.718
$k = 16$	(0.9684, −1.0, 1.3521, −0.5, 2.9094)	11.718
$k = 20$	(1.0, −1.0, 1.3521, −0.5, 3.0)	12.390

The common features were that λ, which controlled the radius of the buoy, tended to reach the upper bound, $\alpha = 1$, which controlled the shape of the bottom of the buoy. Among the different features shown in Tables 3 and 4, β, which controlled the buoy draft, converged to the upper limit of the constraint with the smallest buoy draft, while, shown in Table 5, β converged to the lower limit of the constraint with the largest buoy draft. In order to clarify the variation of wet surface area and drainage volume of the buoy, $C = 0$ in Table 3 was selected for the analysis. In Figure 13, (a) shows the variation of buoy draft volume V with the number of iterations in Table 3 and (b) shows the variation of wet surface area A of the buoy with the number of iterations in Table 3. It can be seen that, in general, the volume of the draft from the buoy, V, decreased with the number of iterations, increased at step 6 of the iteration, and continued to decrease after step 6, while the wet surface area of the buoy, A, increased with the number of iterations. In order to analyze the change in buoy shape during the iterative process, two dimensionless variables, η and φ, were defined. η was the absolute value of the ratio of β to λ, which characterized the flatness of the buoy, with a smaller η indicating a flatter buoy and vice versa. φ was the absolute value of the ratio of α to β, which characterized the taper of the buoy, with a smaller φ indicating a more tapered buoy. The expressions are as follows:

$$\eta = \left| \frac{\beta}{\lambda} \right| \tag{14}$$

$$\varphi = \left| \frac{\alpha}{\beta} \right| \tag{15}$$

Figure 14 below shows the curves for φ and η. As shown, the η curve showed a decreasing trend, indicating that the shape of the buoy became flatter and flatter with the number of iterations, while the φ curve showed a rapid increase after a small decrease at the $5 - th$ iterations, indicating that the shape of the buoy became less tapered with the number of iterations.

Summing up the above patterns, the following can be concluded:

(1) With the shape vector constraint, the wet surface area of the buoy became larger and the drainage volume decreased as the buoy shape was optimized iteratively.
(2) With the shape vector constraint, the buoy shape tended to be flat with a small taper as the buoy shape was optimized iteratively.

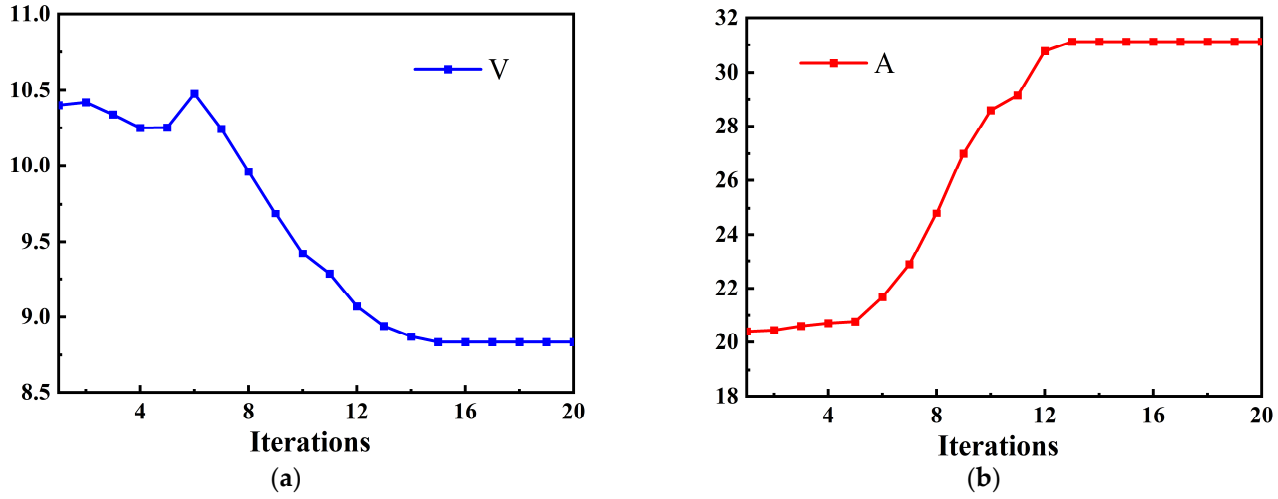

Figure 13. Iterative curves of characteristic parameters: (**a**) draft volume variation curve; (**b**) wet surface area variation curve.

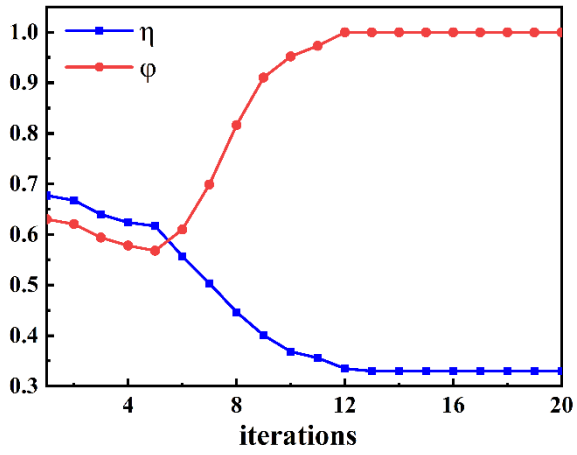

Figure 14. Buoy taper and flatness variation curve.

4. Experimental Validation

To validate the correctness of the optimization method described above, a wave tank experiment was conducted at the Yantai Research Institute of Harbin Engineering University. The experimental setup is depicted in Figure 15. A high-speed camera was employed to capture the buoy's instantaneous motion characteristics, while displacement sensors were utilized to measure the buoy's motion response. The internal clear space dimensions of the wave tank were 10 m × 0.8 m × 0.8 m. The wave tank had the capability for active wave generation, with a maximum operational water depth of 0.6 m or more. When generating regular waves, the wave periods ranged from 0.5 to 2 s, and the maximum wave amplitudes ranged from 30 to 200 mm.

Based on the dimensions of the wave tank, two scaled-down buoys were manufactured with a scale ratio of 0.05. The connection between the buoys and the arm was established through bolts, while the connection between the tower and the arm was facilitated by two bearings. In the experiments, regular waves were generated with a wave period set at 1.03 s and a wave height of 0.06 m. The experimental results are depicted in Figure 16.

The experimental results from the wave tank under scaled conditions clearly indicate a significant difference in the hydrodynamic performance between the scaled-down optimal buoy and the traditional cone buoy. Once the system reached stability, the motion response exhibited a consistent pattern. The swing amplitude of the optimal buoy reached approximately 40 mm, while that of the cone buoy was only 10 mm. This demonstrates

that the hydrodynamic performance of the optimal buoy surpasses that of the cone buoy, thereby validating the effectiveness of the optimization method proposed in this study.

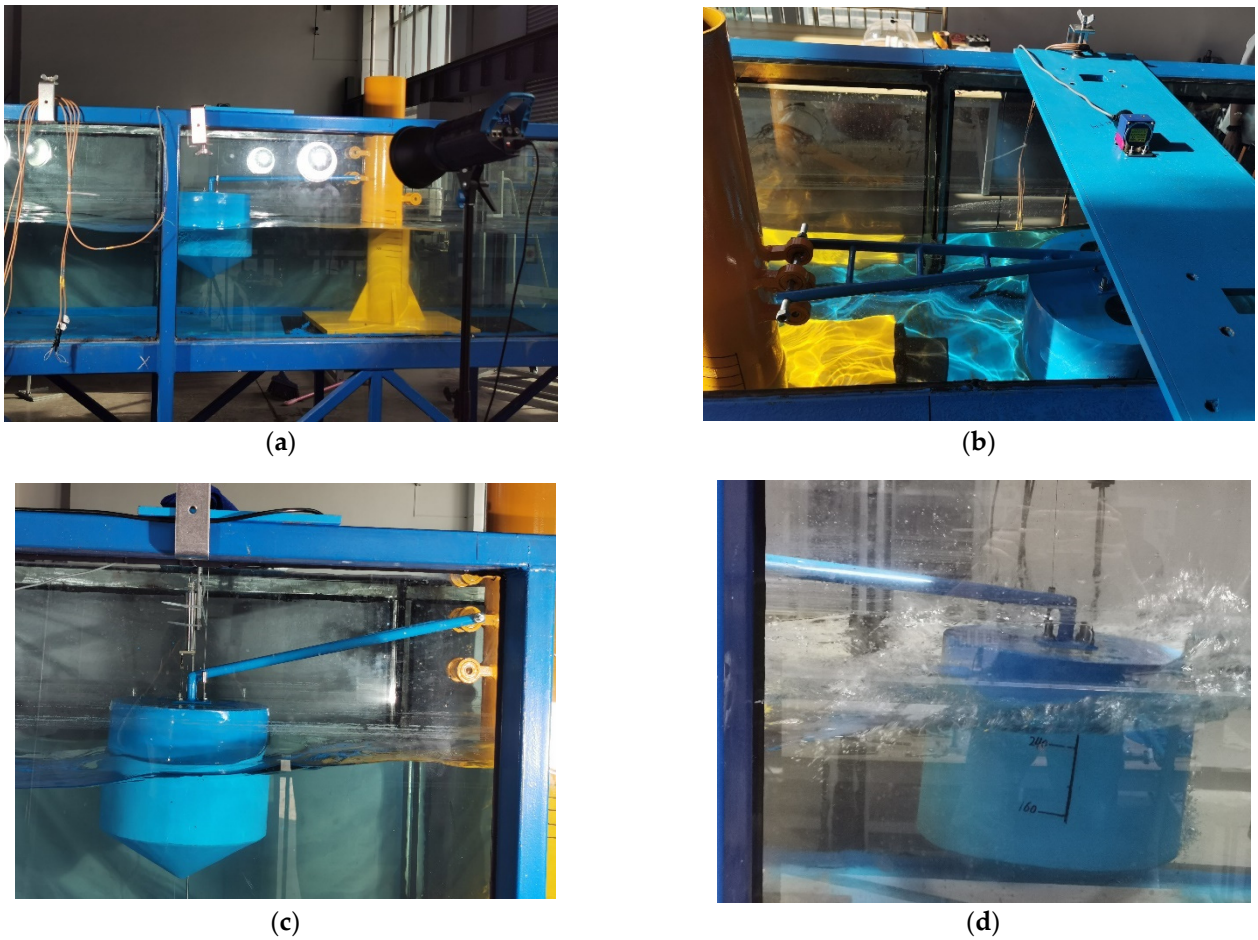

Figure 15. Experimental layouts: (**a**) high-speed camera setup; (**b**) Sensor setup; (**c**) buoy at rest; (**d**) buoy oscillation State.

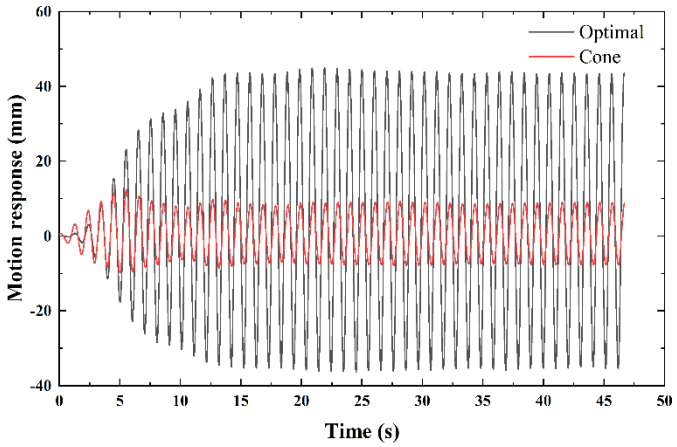

Figure 16. Experimental results.

5. Conclusions

In this paper, an approach to optimizing buoy shape using a PSO algorithm was established, mainly discussing the change in buoy shape during the iterative process with irregular waves, with constant C_{PTO} and different C. The aim was to analyze the effect

of the motion response of the buoy and then summarize the discipline of buoy shape optimization. The optimal buoy shape was compared with the conventional cone buoy shape for hydrodynamic performance and, finally, experimental verification was conducted, which is summarized as follows:

(1) The buoy shape tended to be flatter and less tapered as the objective function increased with increasing values of the upper and lower limits of the coordinates.
(2) The buoy shape tended to decrease the drainage volume and increase the wet surface area.
(3) The optimal buoy shape had better hydrodynamic performance. Through experimental testing, differences in the hydrodynamic performance of the buoys were obtained, thereby validating the effectiveness of the buoy shape optimization method.

Author Contributions: Conceptualization, Y.J.; Methodology, Y.J.; Investigation, H.C.; Data curation, S.H.; Writing—original draft, W.G. and S.H.; Writing—review & editing, S.J.; Funding acquisition, H.L. All authors have read and agreed to the published version of the manuscript.

Funding: This study was supported by the National Natural Science Foundation of China (U2006229, 52101306), Key Research and Development Program of Shandong Province, China (2022CXGC020509), Fundamental Research Funds for the Central Universities (3072022QBZ2701, 3072022QBZ2702, 3072022JC2701), Strategic Rocket Innovation Fund (ZH2022009), Yantai Growth Drivers Conversion Research Institute, and Yantai Science and Technology Achievement Transfer and Transformation Demonstration Base (YTDNY20220425-01).

Institutional Review Board Statement: Not applicable.

Informed Consent Statement: Not applicable.

Data Availability Statement: The data presented in this study are available on request from the corresponding author. The data are not publicly available due to the fact that the dataset production is part of the innovation point of this paper.

Acknowledgments: The authors gratefully acknowledge the financial support mentioned above.

Conflicts of Interest: Authors Wei Ge and Shui Ji were employed by the company State Power Investment Company Science and Technology Research Institute. The remaining authors declare that the research was conducted in the absence of any commercial or financial relationships that could be construed as a potential conflict of interest.

References

1. Falcão, A.F.D.O. Wave energy utilization: A review of the technologies. *Renew. Sustain. Energy Rev.* **2010**, *14*, 899–918. [CrossRef]
2. Babarit, A. On the park effect in arrays of oscillating wave energy converters. *Renew. Energy* **2013**, *58*, 68–78. [CrossRef]
3. Ochs, m.E.; Bull, D.L.; Laird, D.L.; Jepsen, R.A.; Boren, B. *Technological Cost-Reduction Pathways for Point Absorber Wave Energy Converters in the Marine Hydrokinetic Environment*; Sandia National Laboratories: Albuquerque, NM, USA, 2013; 48p.
4. McCabe, A.P. Constrained optimization of the shape of a wave energy collector by genetic algorithm. *Renew. Energy* **2013**, *51*, 274–284. [CrossRef]
5. McCabe, A.P.; Aggidis, G.A.; Widden, m.B. Optimizing the shape of a surge-and-pitch wave energy collector using a genetic algorithm. *Renew. Energy* **2010**, *35*, 2767–2775. [CrossRef]
6. Garcia-Teruel, A.; DuPont, B.; Forehand, D.I.M. Hull geometry optimisation of wave energy converters: On the choice of the optimisation algorithm and the geometry definition. *Appl. Energy* **2020**, *280*, 115952. [CrossRef]
7. Garcia-Teruel, A.; Forehand, D.I.M. Manufacturability considerations in design optimisation of wave energy converters. *Renew. Energy* **2022**, *187*, 857–873. [CrossRef]
8. Abdelkhalik, O.; Coe, R.G.; Bacelli, G.; Wilson, D.G. WEC geometry optimization with advanced control. In Proceedings of the 36th ASME International Conference on Ocean, Offshore and Arctic Engineering, Trondheim, Norway, 25–30 June 2017.
9. Zheng, X.; Ji, m.; Jing, F.; Lu, Y.; Zheng, W.; Zhou, S.; Li, X.; Yan, H. Sea trial test on offshore integration of an oscillating buoy wave energy device and floating breakwater. *Energy Convers. Manag.* **2022**, *256*, 115375. [CrossRef]
10. Reabroy, R.; Zheng, X.; Zhang, L.; Zang, J.; Yuan, Z.; Liu, m.; Sun, K.; Tiaple, Y. Hydrodynamic response and power efficiency analysis of heaving wave energy converter integrated with breakwater. *Energy Convers. Manag.* **2019**, *195*, 1174–1186. [CrossRef]
11. Homayoun, E.; Ghassemi, H.; Ghafari, H. Power Performance of the Combined Monopile Wind Turbine and Floating Buoy with Heave-type Wave Energy Converter. *Pol. Marit. Res.* **2019**, *26*, 107–114. [CrossRef]

12. Kim, S.-J.; Koo, W.; Kim, m.-H. The effects of geometrical buoy shape with nonlinear Froude-Krylov force on a heaving buoy point absorber. *Int. J. Nav. Archit. Ocean Eng.* **2021**, *13*, 86–101. [CrossRef]
13. Berenjkoob, m.N.; Ghiasi, m.; Soares, C.G. Influence of the shape of a buoy on the efficiency of its dual-motion wave energy conversion. *Energy* **2021**, *214*, 118998. [CrossRef]
14. Lin, W.; Shanab, B.H.; Lenderink, C.; Zuo, L. Multi-objective Optimization of the Buoy Shape of an Ocean Wave Energy Converter using Neural Network and Genetic Algorithm. *IFAC PapersOnLine* **2022**, *55*, 145–150. [CrossRef]
15. Wan, Z.; Li, Z.; Zhang, D.; Zheng, H. Design and Research of Slope-Pendulum Wave Energy Conversion Device. *J. Mar. Sci. Eng.* **2022**, *10*, 1572. [CrossRef]
16. Choiniere, m.; Davis, J.; Nguyen, N.; Tom, N.; Fowler, m.; Thiagarajan, K. Hydrodynamics and load shedding behavior of a variable-geometry oscillating surge wave energy converter (OSWEC). *Renew. Energy* **2022**, *194*, 875–884. [CrossRef]
17. Rajagopalan, K.; Cross, P.; Ulm, N.; Ravikumar, S.; Das, T.; Prabhu, m.; Chaudhuri, A.; Samad, A. Compact Wave Powered Desalination Unit. In Proceedings of the OCEANS 2022—Chennai, Chennai, India, 21–24 February 2022; pp. 1–7.
18. Nazari Berenjkoob, m.; Ghiasi, m.; Guedes Soares, C. On the improved design of the buoy geometry on a two-body wave energy converter model. *J. Renew. Sustain. Energy* **2019**, *11*, 054702. [CrossRef]
19. Shadman, m.; Estefen, S.F.; Rodriguez, C.A.; Nogueira, I.C.M. A geometrical optimization method applied to a heaving point absorber wave energy converter. *Renew. Energy* **2018**, *115*, 533–546. [CrossRef]
20. Wen, Y.; Wang, W.; Liu, H.; Mao, L.; Mi, H.; Wang, W.; Zhang, G. A Shape Optimization Method of a Specified Point Absorber Wave Energy Converter for the South China Sea. *Energies* **2018**, *11*, 2645. [CrossRef]
21. Tao, J.; Cao, F.; Dong, X.; Li, D.; Shi, H. Optimized design of 3-DOF buoy wave energy converters under a specified wave energy spectrum. *Appl. Ocean Res.* **2021**, *116*, 102885. [CrossRef]
22. Yang, J.; Zhang, D.-h.; Chen, Y.; Liang, H.; Tan, m.; Li, W.; Ma, X.-d. Design, optimization and numerical modelling of a novel floating pendulum wave energy converter with tide adaptation. *China Ocean Eng.* **2017**, *31*, 578–588. [CrossRef]
23. Alamian, R.; Shafaghat, R.; Safaei, m.R. Multi-Objective Optimization of a Pitch Point Absorber Wave Energy Converter. *Water* **2019**, *11*, 969. [CrossRef]
24. Esmaeilzadeh, S.; Alam, m.-R. Shape optimization of wave energy converters for broadband directional incident waves. *Ocean Eng.* **2019**, *174*, 186–200. [CrossRef]
25. Amini, E.; Golbaz, D.; Asadi, R.; Nasiri, m.; Ceylan, O.; Majidi Nezhad, m.; Neshat, m. A Comparative Study of Metaheuristic Algorithms for Wave Energy Converter Power Take-Off Optimisation: A Case Study for Eastern Australia. *J. Mar. Sci. Eng.* **2021**, *9*, 490. [CrossRef]
26. Song, m.; Liu, S.; Li, W.; Chen, S.; Li, W.; Zhang, K.; Yu, D.; Liu, L.; Wang, X. A Continuous Space Location Model and a Particle Swarm Optimization-Based Heuristic Algorithm for Maximizing the Allocation of Ocean-Moored Buoys. *IEEE Access* **2021**, *9*, 32249–32262. [CrossRef]
27. He, Z.; Ning, D.; Gou, Y.; Zhou, Z. Wave energy converter optimization based on differential evolution algorithm. *Energy* **2022**, *246*, 123433. [CrossRef]
28. Liu, T.; Liu, Y.; Huang, S.; Xue, G. Shape Optimization of Oscillating Buoy Wave Energy Converter Based on the Mean Annual Power Prediction Model. *Energies* **2022**, *15*, 7470. [CrossRef]
29. Ahamed, R.; McKee, K.; Howard, I. Advancements of wave energy converters based on power take off (PTO) systems: A review. *Ocean Eng.* **2020**, *204*, 107248. [CrossRef]
30. Baninajar, H.; Modaresahmadi, S.; Wong, H.Y.; Bird, J.Z.; Williams, W.; DeChant, B.; Southwick, P. A Dual-Stack Coaxial Magnetic Gear for a Wave Energy Conversion Generator. *IEEE Trans. Magn.* **2022**, *58*, 1–12. [CrossRef]
31. Liu, Y.; Yu, H.; Zhang, Q. Research on Permanent Magnet-Induction Magnetic Screw for Wave Energy Conversion. In Proceedings of the 2022 IEEE 20th Biennial Conference on Electromagnetic Field Computation (CEFC), Virtually, 24–26 October 2022; pp. 1–2.
32. Calvário, m.; Gaspar, J.F.; Kamarlouei, m.; Hallak, T.S.; Guedes Soares, C. Oil-hydraulic power take-off concept for an oscillating wave surge converter. *Renew. Energy* **2020**, *159*, 1297–1309. [CrossRef]
33. Fan, Y.; Mu, A.; Ma, T. Design and control of a point absorber wave energy converter with an open loop hydraulic transmission. *Energy Convers. Manag.* **2016**, *121*, 13–21. [CrossRef]
34. Geng, D.; Zheng, Y.; Chen, Q.; Yue, X.; Yan, D. Novel hydraulic mechanism-based output power regulation for the wave energy converter. *Appl. Ocean Res.* **2021**, *110*, 102587. [CrossRef]
35. Veurink, m.G.; Weaver, W.W.; Robinett, R.D.; Wilson, D.G.; Matthews, R.C. Efficient WEC Array Buoy Placement optimization with Multi-Resonance Control of the Electrical Power Take-off for Improved Performance. In Proceedings of the OCEANS 2022, Hampton Roads, VI, USA, 17–20 October 2022; pp. 1–6.
36. De Andrés, A.D.; Guanche, R.; Meneses, L.; Vidal, C.; Losada, I.J. Factors that influence array layout on wave energy farms. *Ocean Eng.* **2014**, *82*, 32–41. [CrossRef]
37. Stratigaki, V.; Troch, P.; Stallard, T.; Forehand, D.; Kofoed, J.; Folley, m.; Benoit, m.; Babarit, A.; Kirkegaard, J. Wave Basin Experiments with Large Wave Energy Converter Arrays to Study Interactions between the Converters and Effects on Other Users in the Sea and the Coastal Area. *Energies* **2014**, *7*, 701–734. [CrossRef]
38. Kennedy, J.; Eberhart, R. Particle swarm optimization. In Proceedings of the ICNN'95—International Conference on Neural Networks, Perth, Australia, 27 November–1 December 1995; Volume 1944, pp. 1942–1948.

39. Piotrowski, A.P.; Napiorkowski, J.J.; Piotrowska, A.E. Population size in Particle Swarm Optimization. *Swarm Evol. Comput.* **2020**, *58*, 100718. [CrossRef]
40. Shi, Y.; Eberhart, R. A modified particle swarm optimizer. In Proceedings of the 1998 IEEE International Conference on Evolutionary Computation Proceedings. IEEE World Congress on Computational Intelligence (Cat. No.98TH8360), Anchorage, AK, USA, 4–9 May 1998; pp. 69–73.
41. Clerc, m. The swarm and the queen: Towards a deterministic and adaptive particle swarm optimization. In Proceedings of the 1999 Congress on Evolutionary Computation-CEC99 (Cat. No. 99TH8406), Washington, DC, USA, 6–9 July 1999; Volume 1953, pp. 1951–1957.
42. Shi, Y. Particle swarm optimization: Developments, applications and resources. In Proceedings of the 2001 Congress on Evolutionary Computation (IEEE Cat. No.01TH8546), Seoul, South Korea, 27–30 May 2001; Volume 81, pp. 81–86.
43. Ruehl, K.; Michelen, C.; Kanner, S.; Lawson, m.; Yu, Y.H. Preliminary verification and validation of wec-sim, an open-source wave energy converter design tool. In Proceedings of the 33rd ASME International Conference on Ocean, Offshore and Arctic Engineering, San Francisco, CA, USA, 8–13 June 2014.
44. Goda, Y. Overview on the applications of random wave concept in coastal engineering. *Proc. Jpn. Acad. Ser. B* **2008**, *84*, 374–385. [CrossRef] [PubMed]
45. Liang, B.; Liu, X.; Li, H.; Wu, Y.; Lee, D. Wave Climate Hindcasts for the Bohai Sea, Yellow Sea, and East China Sea. *J. Coast. Res.* **2014**, *32*, 172–180. [CrossRef]